Magnetic Resonance Imaging 71 (2020) 161–169

Contents lists available at ScienceDirect

Magnetic Resonance Imaging

journal homepage: www.elsevier.com/locate/mri

Original contribution

The comparison of high-resolution diffusion weighted imaging (DWI) with high-resolution contrast-enhanced MRI in the evaluation of breast cancers

Ayami Ohno Kishimoto[a], Masako Kataoka[a,*], Mami Iima[a,b], Maya Honda[a], Kanae Kawai Miyake[a], Akane Ohashi[a], Rie Ota[a], Tatsuki Kataoka[c], Takaki Sakurai[c], Masakazu Toi[d], Kaori Togashi[a]

[a] Department of Diagnostic Imaging and Nuclear Medicine, Graduate School of Medicine, Kyoto University, 54 Shogoin-Kawaharacho, Sakyo-ku, Kyoto 606-8507, Japan
[b] Institute for Advancement of Clinical and Translational Science (iACT), Kyoto University Hospital, 54 Shogoin-Kawaharacho, Sakyo-ku, Kyoto 606-8507, Japan
[c] Department of Diagnostic Pathology, Kyoto University Hospital, 54 Shogoin-Kawaharacho, Sakyo-ku, Kyoto 606-8507, Japan
[d] Department of Breast Surgery, Kyoto University Hospital, 54 Shogoin-Kawaharacho, Sakyo-ku, Kyoto 606-8507, Japan

ARTICLE INFO

Keywords:
Magnetic resonance imaging
Breast neoplasms
High-resolution
Diffusion-weighted imaging
Non-mass lesions

ABSTRACT

Purpose: We sought to investigate the performance of high resolution (HR) diffusion-weighted imaging (DWI) using readout-segmented echo-planar imaging (rs-EPI), compared with high-resolution contrast-enhanced MRI (HR CE-MRI) in terms of morphological accuracy, on the basis of the Breast Imaging and Reporting and Data System (BI-RADS) MRI descriptors and lesion size.

Methods: This retrospective study included the image data of 94 patients with surgically confirmed malignant breast lesions who had undergone high resolution diffusion-weighted imaging (HR-DWI) and HR CE-MRI. Two radiologists blinded to the final diagnosis independently identified the lesions on HR-DWI, described the morphology of the lesions according to BI-RADS descriptors, and measured lesion size. HR CE-MRI was subsequently evaluated using the same procedure. The inter-method agreement of the morphology was assessed using kappa statistics. Correlation on size was also assessed.

Results: Reader A detected 79 mass lesions and 37 non-mass lesions on HR-DWI and HR CE-MRI. Reader B detected 81 mass lesions and 33 non-mass lesions on HR-DWI and HR CE-MRI. Very high agreement (kappa = 0.81–0.89, $p < .05$) was observed in the shape and margin assessment of mass lesions, where agreement on internal enhancement/signals was moderate to substantial (kappa = 0.43–0.61, $p < .05$). Disagreement was mostly seen in the evaluation of rim enhancement. High agreement was observed for non-mass lesion distribution (kappa = 0.76–0.84, $p < .05$), and agreement on internal enhancement/signals was moderate to fair (kappa = 0.34–0.49, $p < .05$). Agreement among heterogeneous, clumped, and clustered-ring patterns was variable. Size assessment showed very strong correlation both in mass (Spearman's rho = 0.90–0.96, $p < .0001$) and non-mass lesions (Spearman's rho = 0.86, $p < .0001$).

Conclusions: The findings in morphology and lesion extent showed high agreement between HR-DWI and HR CE-MRI for malignant breast lesions. These results imply the potential of applying HR-DWI for evaluation of malignant breast lesions using BI-RADS MRI.

1. Introduction

Dynamic contrast-enhanced MRI (DCE-MRI) is the gold standard in evaluation of breast lesions [1]. Morphological assessment plays an important role in the decision-making process in the evaluation of breast tumors [2–5]. Thus, morphological description in addition to kinetic assessment were adopted by the American College of Radiology Breast Imaging and Reporting and Data System (BI-RADS) MRI 2013, which is widely used in evaluating and describing breast lesions [1]. Improved morphological evaluation is now available using high-resolution contrast-enhanced MRI (HR CE-MRI), with increased spatial resolution of <1 mm [6]. However, its specificity is highly variable,

Abbreviations: BI-RADS, American College of Radiology Breast Imaging and Reporting and Data System; DCIS, ductal carcinoma *in situ*; DWI, diffusion-weighted imaging; HR, high resolution; HR CE-MRI, high resolution contrast-enhanced MRI; HR-DWI, high resolution diffusion-weighted imaging; IDC, invasive ductal carcinoma; NST, no special type; RESOLVE, readout segmentation of long variable echo-trains; rs-EPI, readout-segmented echo-planar imaging; SNR, signal-to-noise ratio; ss-EPI, single-shot echo-planar imaging; 3D-VIBE, three-dimensional volumetric interpolated breath-hold examination

* Corresponding author.
E-mail address: makok@kuhp.kyoto-u.ac.jp (M. Kataoka).

https://doi.org/10.1016/j.mri.2020.03.007
Received 19 November 2019; Received in revised form 28 February 2020; Accepted 25 March 2020

which may lead to unnecessary biopsy.

The assessment of breast lesions using BI-RADS is based on DCE-MRI, using a gadolinium contrast agent. However, in addition to the potential risk of nephrogenic systemic fibrosis in cases with renal impairment [7], its deposition in the brain after cumulative loads has led to controversy over its possible long-term effects on the body [8–11]. This is problematic in high-risk screening or follow-up studies in neoadjuvant chemotherapy, where repeated examinations are inevitable. A similarly accurate evaluation without contrast enhancement would be ideal.

Diffusion-weighted imaging (DWI) is now a well-established non-contrast imaging technique, which is commonly added to routine breast MRI sequences in daily clinical imaging, and apparent diffusion coefficient (ADC) has been a well-established quantitative measurement for differentiation of benign and malignant breast lesions, although it is not included in the assessment in BI-RADS MRI [12,13]. Diffusion of water molecules tends to be hindered or restricted in malignant breast tumors due to higher cellularity, resulting in high intensity on DWI with low ADC values [14,15]. This technique increases specificity [13], and may potentially supplement DCE-MRI. Single-shot echo-planar imaging (ss-EPI) is a well-established conventional method for the acquisition of DWI data with short scan times; however, it suffers from geometric distortion, signal dropout, and image blurring [16]. An alternative imaging technique, readout-segmented echo-planar imaging (rs-EPI) with a navigator echo scheme, was developed to acquire high-resolution diffusion-weighted imaging (HR-DWI) with lower geometric distortion and artifacts. Rs-EPI is a multi-shot sequence that reduces susceptibility artifact and blurring arising from T2* decay. This method allows for HR-DWI with nearly 1-mm spatial resolution [17]. The acquisition time for rs-EPI is a few minutes longer than that for ss-EPI; however, the distortion is improved [18,19]. Its efficacy has already been reported in some regions, including skull base and head and neck [20,21]. The advantage of rs-EPI in breast diagnosis has been reported as well [22–24].

Now that we have the ability to perform HR-DWI with spatial resolution close to that of HR CE-MRI, we hypothesized that HR-DWI may allow accurate morphological evaluation in malignant breast lesions equal to that of HR CE-MRI. As morphological assessment of breast lesions on DWI has not been established so far, we have investigated how breast lesions to be appreciated in terms of BI-RADS lexicons on HR-DWI. A preliminary study comparing HR-DWI and HR CE-MRI in breast lesion extent showed high correlation for mass-type lesions [25]. Here, with a larger population, we aimed to examine the performance of HR-DWI using rs-EPI compared with HR CE-MRI in terms of morphological assessment using BI-RADS-MRI descriptors in addition to lesion size assessment. We also compared the lesion size between HR-DWI and HR CE-MRI.

2. Materials and methods

2.1. Study population

Our Institutional Review Board approved this retrospective study, and the need for written informed consent was waived. HR-DWI using rs-EPI and HR CE-MRI have been acquired as part of our clinical routine MR protocol for pre-treatment evaluation of known breast cancer or a suspicious breast lesion. Between July 2015 and March 2018, 275 consecutive patients who underwent breast MRI including HR-DWI using rs-EPI with subsequent surgical confirmation of malignancy were included in this study. The number of patients included in this study has been analyzed previously [19]. In the prior study in a different context, we aimed to investigate the accuracy of HR-DWI in visualizing malignant breast lesions and evaluating their extent comparing with pathology. In this study, we focused on the evaluation using BI-RADS lexicon and compared HR-DWI with contrast-enhanced images. Exclusion criteria were those who did not undergo contrast-enhanced imaging and those who were receiving neoadjuvant chemotherapy or hormonal therapy prior to surgery.

Table 1
Pathology of the lesions.

Pathological type	N (%)
Invasive carcinoma NST	66 (70.2)
DCIS	11 (11.7)
Mucinous carcinoma	5 (5.3)
ILC	5 (5.3)
Apocrine carcinoma	2 (2.1)
Invasive papillary carcinoma	1 (1.1)
Intraductal papillary carcinoma	1 (1.1)
Solid papillary carcinoma	1 (1.1)
Invasive micropapillary carcinoma	1 (1.1)
Adenoid cystic carcinoma	1 (1.1)
Total	94 (100.0)

DCIS = ductal carcinoma *in situ*; ILC = invasive lobular carcinoma; NST = no special type.

2.2. Pathology

The final diagnosis based on pathological report was noted on Table 1.

2.3. MRI protocol

A 3 T MRI system (MAGNETOM Prisma: Siemens Healthcare GmbH, Erlangen, Germany) and a dedicated 18-channel breast coil (Siemens Healthcare GmbH, Erlangen, Germany) were used for image acquisition. The MRI protocol included HR-DWI using rs-EPI at b = 0 and 850 s/mm^2 (unilateral, over the breast with the known/suspected lesion); sagittal orientation, TR/TE = 8300/48 ms; FOV, 180 × 145 mm; matrix, 166 × 107; acquired voxel size, 1.1 × 1.4 × 1.5 mm; 45 sections; total acquisition time, 5 min 15 s . (Phase direction of images was obtained with 80% phase resolution and reconstructed into matrix of 166 × 134; reconstructed voxel size 1.1× 1.1× 1.5 mm.) HR CE-MRI (both breasts; coronal orientation; three-dimensional volumetric interpolated breath-hold examination (3D-VIBE) with fat suppression; TR/TE = 4.61/1.80 ms; FA, 15; FOV, 330 × 330 mm; matrix, 512 × 461; acquired voxel size, 0.6 × 0.7 × 0.8 mm; 176 sections; total acquisition time, 2 min 26 s) obtained 2–5 min after the administration of contrast agent, with sagittal reconstruction. (Phase direction of images was obtained with 90% phase resolution and reconstructed into matrix of 512 × 512; reconstructed voxel size 0.6 × 0.6 × 0.8 mm.) For HR-DWI, we used readout segmentation of long variable echo-trains (RESOLVE) sequence for rs-EPI and the scan protocol was designed to be nearly isovoxel, with voxel size as small as possible while keeping sufficient signal-to-noise ratio (SNR).

2.4. Image interpretation and analysis

Images were interpreted using a workstation (Aquarius NET Viewer; TeraRecon, Foster City, CA, USA). Two board-certified radiologists specializing in breast imaging (reader A with nine years and reader B with 20 years of experience) independently read HR-DWI images and ADC maps and identified breast lesions suspicious for malignancy. They had been informed that each patient had one or more malignant lesions but were blinded to the final diagnosis including the number and location of lesions, and the detailed pathological information.

Two readers first identified and evaluated the lesions on HR-DWI alone, blind to other images. Those lesions with lack of visibility on HR-DWI were not included in the analysis. Each reader recorded the location of the lesions based on BI-RADS when reading HR-DWI. The evaluation was performed based on BI-RADS descriptors in which kinetic assessment was substituted for the qualitative evaluation of DWI

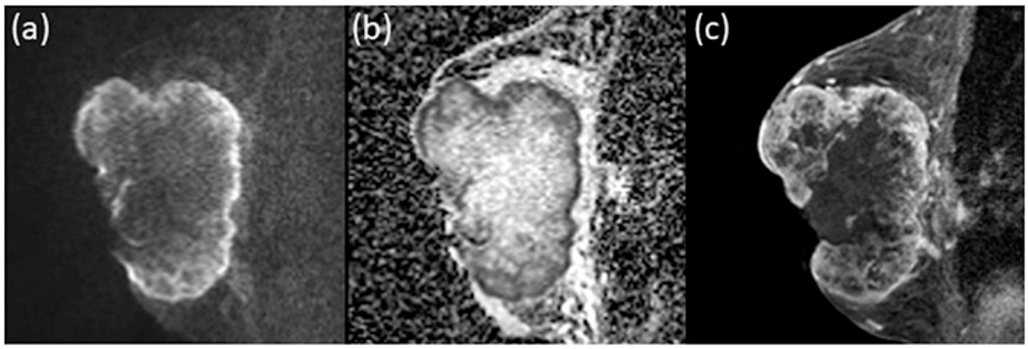

Fig. 1. Malignant mass lesion in an 85-year-old patient.
(a) HR-DWI (b = 850 s/mm^2), (b) ADC map, (c) HR CE-MRI.
(a, b) A mass lesion with high-signal rim on HR-DWI (b = 850 s/mm^2) with low values on ADC map. (c) The lesion was detected on HR CE-MRI. Both readers classified it as a mass lesion on both methods. Reader A measured it as 61 mm on HR-DWI and 67 mm on HR CE-MRI, while reader B measured it as 63 mm on HR-DWI and 64 mm on HR CE-MRI. Both readers diagnosed the lesion with an irregular shape, poorly circumscribed margins and high signal in rim shape/rim enhancement on both methods. The pathological diagnosis was adenoid cystic carcinoma.

signals, that is, lesions with high intensity on HR-DWI and low values on the ADC map were interpreted as suspicious. Lesion conspicuity was quantified with a 4-point scale based on signal contrast between lesions and breast tissue: 1 = poor, 2 = average, 3 = good, 4 = excellent. The lesions were classified into mass lesions or non-mass lesions by two readers. In case of mixed lesions containing mass and non-mass components, each reader evaluated the mass components as “mass lesions” and non-mass components as “non-mass lesions” separately. Image analysis was performed on each lesion. Two readers assessed the morphology of lesions based on the BI-RADS descriptors, using “elevated signal” instead of “enhancement”. Two readers subsequently measured the diameters of the lesions in the anterior-posterior direction (A-P diameters) in the selected slice in the sagittal plane which contained the largest section of the lesion on HR-DWI. After reading each HR-DWI, they evaluated HR-DWI-detected lesions on HR CE-MRI examination. Each reader checked the locations of the lesions recorded on HR-DWI when reading HR CE-MRI and identified the correlated lesions. Lesion conspicuity was qualified, the morphology was evaluated using BI-RADS-MRI and the diameters of the lesion in A-P direction were measured.

2.5. Statistical analysis

Inter-method agreement between HR-DWI and HR CE-MRI was assessed in terms of morphology for two readers. Correlation on size was also assessed.

Kappa statistics for morphology descriptor subcategory were calculated. Using a scale by Viera and Garret, a kappa statistic of ≤ 0.2 was considered slight agreement; 0.21–0.40, fair agreement; 0.41–0.60, moderate agreement; 0.61–0.80, substantial agreement; and 0.81–0.99, almost perfect agreement [26].

The Wilcoxon signed-rank test was performed to assess if lesion size measurements were significantly different between the two methods. Bland–Altman assessment was used to compare the agreement between lesion measurements on HR-DWI and HR CE-MRI by two readers, regarding mass lesions and non-mass lesions. The correlation between lesion diameters on HR-DWI and on HR CE-MRI was evaluated using Spearman's correlation coefficient, owing to the non-normal distribution of lesion size. The level of Spearman's correlation coefficient was defined as follows: very strong, $r = 1.0–0.8$; moderately strong, $r = 0.8–0.6$; fair, $r = 0.5–0.3$; and poor, $r < 0.3$ [27].

All tests were two-sided, with $p < .05$ indicating significance. Statistical analysis was performed with JMP Pro 14 (SAS Institute, Cary, NC, USA) and STATA ver. 13.1 (StataCorp, College Station, TX, USA).

3. Results

3.1. Study population

Out of 275 cases undergoing HR-DWI with subsequently proven malignant lesions through surgery, 181 cases were excluded as 171 patients received neoadjuvant chemotherapy or hormonal therapy prior to surgery and 10 patients underwent non-contrast enhanced imaging. 94 consecutive cases (all female, mean age 60.2 y; range 32–85 y) were finally included in the analysis. Detailed final diagnosis based on pathological reports is summarized in Table 1.

3.2. Lesion evaluations

Out of 94 cases without pathological information, Reader A detected 79 mass lesions and reader B detected 81 mass lesions on HR-DWI. Reader A detected 37 non-mass lesions and reader B detected 33 non-mass lesions on HR-DWI. Then, readers confirmed these lesions on HR CE-MRI. In our cases, all the lesions detected on HR-DWI were detected on HR CE-MRI.

3.3. Mass lesions

All the lesions detected as mass lesions on HR-DWI were detected as mass lesions on HR CE-MRI and not detected as non-mass lesions by both readers. For 79 mass lesions reader A detected, the mean and standard deviation (SD) of lesion conspicuity score for HR-DWI was 3.65 ± 0.73 and for HR CE-MRI was 3.85 ± 0.58. For 81 mass lesions reader B detected, the mean and standard deviation (SD) of lesion conspicuity for HR-DWI was 3.54 ± 0.81 and for HR CE-MRI was 3.89 ± 0.42. Examples of a typical case of mass lesion and mixed-type lesion including mass component are shown in Figs. 1, 2 and 3.

The inter-method agreement between the assessment of shape was almost perfect for both readers (kappa = 0.81, 0.89, $p < .001$), and the assessment of margin was almost perfect for reader B (kappa = 0.85, $p < .001$). The kappa coefficient of mass margin could not be calculated for reader A as reader A categorized margin of all the lesions as “non-circumscribed” on HR CE-MRI. The prevalence of “non-circumscribed” was too high to calculate appropriate kappa value [28] (Table 2). The assessment of internal signal/enhancement pattern was moderate for reader A (kappa = 0.43, $p < .001$) and substantial for reader B (kappa = 0.61, $p < .001$).

For internal signal on HR-DWI and enhancement on HR CE-MRI, mismatch in agreement was mostly seen in the lesions with “high signal in rim shape” on HR-DWI and “rim enhancement” on HR CE-MRI. In reader A and B, 22 out of 44 lesions and 29 out of 46 lesions with “rim enhancement” were diagnosed to have “high signal in rim shape” in HR-DWI, for an agreement of 50.0% and 63.0%, respectively. The rest of those lesions with “rim enhancement” were mostly assessed to have heterogeneous signals on HR-DWI by both readers. Reader A identified 35 lesions and Reader B identified 34 lesions with “heterogeneous enhancement”, and their agreement with the HR-DWI was 94.3% (33 lesions) and 100.0% (34 lesions), respectively. The detailed observed morphological features and agreement between HR-DWI and HR CE-MRI are shown in Table 3.

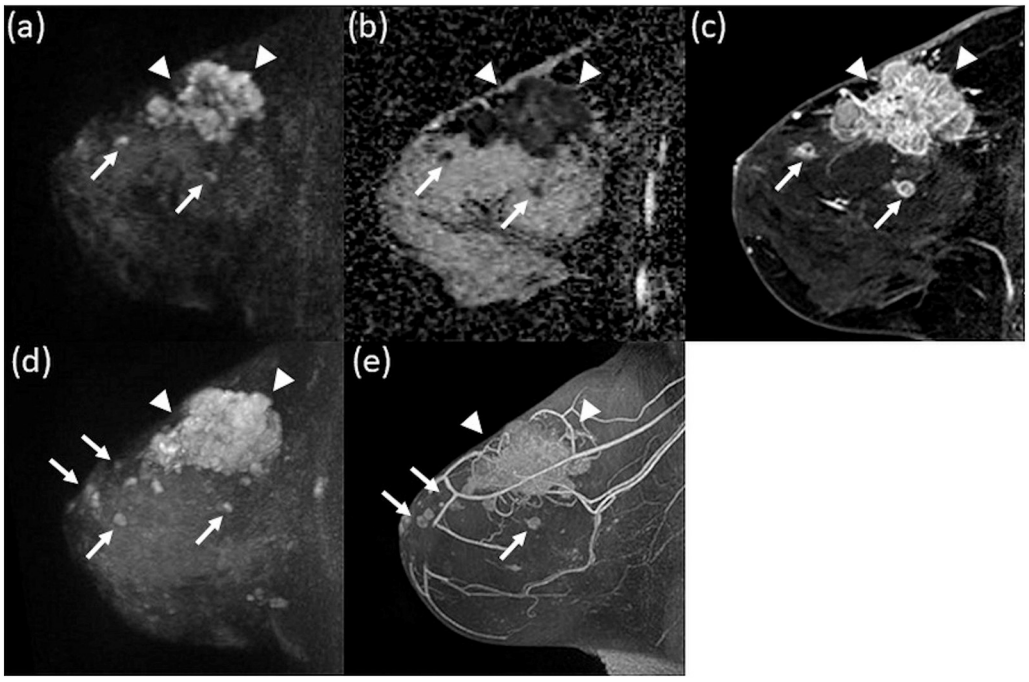

Fig. 2. Malignant mixed-type lesions in a 50-year-old patient.
(a) HR-DWI (b = 850 s/mm^2), (b) ADC map, (c) HR CE-MRI, (d) Maximum intensity projection (MIP) image for HR-DWI, (e) MIP image for HR CE-MRI. (a, b, d) A mass lesion (arrowheads) surrounded by non-mass lesions with clumped pattern (arrows) showed high intensity on HR-DWI with low values on ADC map. (c, e) The lesions were detected on HR CE-MRI.
Both readers classified it as a mass lesion with non-mass lesions on both methods. Reader A measured the mass lesion as 44 mm on HR-DWI and 47 mm on HR CE-MRI, while reader B measured it as 48 mm on both methods. Both readers diagnosed the lesion with irregular shape, poorly circumscribed margins, and high signal in rim shape/rim enhancement on both methods. Reader A measured the non-mass lesion as 63 mm on HR-DWI and 66 mm on HR CE-MRI, while reader B measured it as 66 mm on both methods. Both readers diagnosed the lesions with segmental distribution and a clumped signal/enhancement pattern. Pathological diagnosis was Invasive carcinoma NST.

The mean and SD of AP diameter was 15.0 ± 9.7 mm (range: 5–61 mm) for HR-DWI and 17.3 ± 10.1 mm (range: 6–67 mm) for HR CE-MRI by reader A and 15.7 ± 10.1 mm (range: 4–63 mm) for HR-DWI and 16.8 ± 9.6 mm (range: 6–64 mm) for HR CE-MRI by reader B. The size of mass lesions measured on HR-DWI tended to be smaller than that on HR CE-MRI, however, Wilcoxon signed-rank test showed that the difference was not significant for reader B (p = .035 and p = .19 for readers A and B, Table 4). Bland–Altman plots for measured parameters (Fig. 5, (a) and (b)) showed the agreement between lesion measurements on HR-DWI and HR CE-MRI by two readers. Size difference between HR-DWI and HR CE-MRI was mostly within 10 mm for both readers for mass lesions. Mean and SD of the size differences between HR-DWI and HR CE-MRI were 2.3 ± 2.9 mm for reader A and 1.1 ± 1.8 mm for reader B.

The scatterplot shown in Fig. 6 shows the correlation between HR-DWI and HR CE-MRI in AP diameters for each reader. The Spearman's coefficient in AP diameters was 0.90 for reader A (p < .0001) and 0.96 for reader B (p < .0001), respectively, meaning very strong correlation (Table 4).

3.4. Non-mass lesions

All the lesions detected as non-mass lesions on HR-DWI were detected as non-mass lesions on HR CE-MRI and not detected as mass lesions by both readers. For 37 non-mass lesions reader A detected, the lesion conspicuity for HR-DWI was 2.70 ± 0.85 and for HR CE-MRI was 3.27 ± 0.93. For 33 non-mass lesions reader B detected, the lesion conspicuity for HR-DWI was 2.91 ± 0.77 and for HR CE-MRI was 3.59 ± 0.80. Typical examples of a mixed-type lesion including non-mass component and a non-mass lesion are shown in Figs. 2 and 4. The inter-method agreement between the assessment of distribution was almost perfect for reader A (kappa = 0.84, p < .001) and substantial for reader B (kappa = 0.76, p < .001), and the assessment of internal enhancement was moderate for reader A (kappa = 0.49, p < .001) and

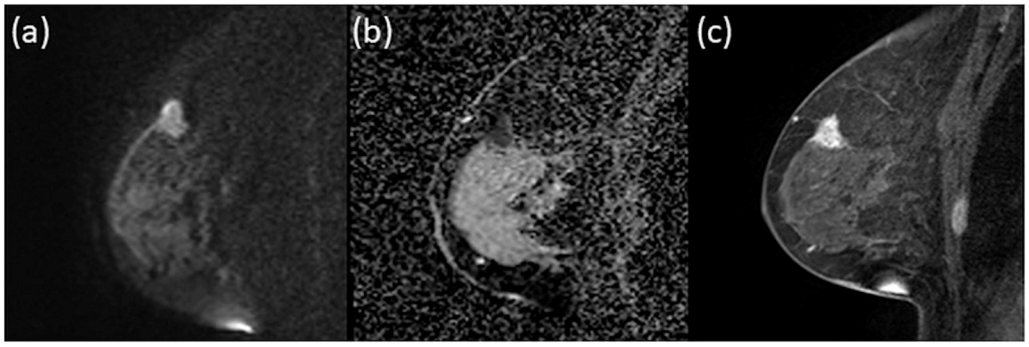

Fig. 3. Malignant mass lesion in a 80-year-old patient.
(a) HR-DWI (b = 850 s/mm^2), (b) ADC map, (c) HR CE-MRI.
(a, b) Mass lesion with high intensity on HR-DWI (b = 850 s/mm^2) with low values on ADC map was detected. (c) The lesion was detected on HR CE-MRI. Both readers classified it as a mass lesion on both methods. Reader A measured it as 9 mm on HR-DWI and 16 mm on HR CE-MRI, while reader B measured it as 11 mm on HR-DWI and 14 mm on HR CE-MRI. Both readers diagnosed the lesion with an irregular shape, poorly circumscribed margins and high signal in rim shape/rim enhancement on both methods. Pathological diagnosis was Invasive carcinoma NST.

Table 2
Intermethod-agreement of lesion morphology between HR-DWI and HR CE-MRI.

Morphology	Reader A				Reader B			
Mass lesions	Number of agreement (%)		K	(p-value)	Number of agreement (%)		K	(p-value)
1) Shape	73/79	(92.4)	0.81	(< 0.05)	76/81	(93.8)	0.89	(< 0.05)
2) Margin	78/79	(98.7)	[a]		80/81	(98.8)	0.85	(< 0.05)
3) Internal enhancement (signal)	55/79	(70.0)	0.43	(< 0.05)	64/81	(79.0)	0.61	(< 0.05)
Non-mass lesions	Number of agreement (%)		K	(p-value)	Number of agreement (%)		K	(p-value)
1) Distribution	34/37	(89.5)	0.84	(< 0.05)	30/33	(90.9)	0.76	(< 0.05)
2) Internal enhancement (signal)	26/37	(68.4)	0.49	(< 0.05)	21/33	(63.6)	0.34	(< 0.05)

[a] Because reader A categorized the margins of all HR CE-MRI lesions as "non-circumscribed", the prevalence of "non-circumscribed" was too high to calculate an appropriate kappa value (Feinsterin AR and Ciccetti DV, 1990 Journal of Clinical Epidemiology 6:p543).

fair for reader B (kappa = 0.34, p = .022), which are shown in Table 2.

Mismatch in agreement on internal signal/enhancement pattern was mostly seen in clustered-ring enhancement detected on HR CE-MRI. Reader A diagnosed six lesions with clustered-ring enhancement, where one lesion (16.7%) was diagnosed to have "clustered-ring signals" in HR-DWI, and the other five lesions were diagnosed as heterogeneous or clumped pattern on HR-DWI. For reader B, none of the 9 lesions with clustered-ring enhancement was diagnosed as "clustered-ring signals" on HR-DWI (0.0%). The detailed observed morphological features and agreement between HR-DWI and HR CE-MRI are shown in Table 3.

The mean and SD of AP diameter were 19.5 ± 14.8 mm (range: 3–63 mm) for HR-DWI and 22.9 ± 14.8 mm (range: 3–66 mm) for HR CE-MRI for reader A and 21.2 ± 13.5 mm (range: 4–66 mm) for HR-DWI and 25.6 ± 14.6 mm (range: 4–66 mm) for HR CE-MRI for reader B. The extent of non-mass lesions measured on HR-DWI had a tendency to be smaller that of HR CE-MRI, however, the Wilcoxon signed-rank test showed the difference was not significant (reader A and reader B showed p = .24 and p = .20, Table 4).

Bland–Altman plots for measured parameters (Fig. 5(c) and (d)) showed the agreement between lesion measurements on HR-DWI and HR CE-MRI by two readers. Mean and SD of the size differences between HR-DWI and HR CE-MRI were 3.5 ± 7.7 mm for reader A and 4.4 ± 7.4 mm for reader B, showing wider range compared to mass lesions.

The scatterplot shown in Fig. 7 demonstrates the correlation between HR-DWI and HR CE-MRI and AP diameters in each reader. The Spearman's coefficient in A-P diameters was 0.86 for both readers (p < .0001).

4. Discussion

Our study showed that HR-DWI and HR CE-MRI showed almost perfect agreement in morphological assessment in shape and margin of mass lesions and substantial to almost perfect agreement in distribution

Table 3
Observed morphological features and correlation between HR-DWI and HR CE-MRI.

Mass lesions		Reader A	N = 79		Reader B	N = 81	
		N (%)		N/CE[a] (%)	N (%)		N/CE[a] (%)
		DWI	CE	Number of agreements	DWI	CE	Number of agreements
Shape	Oval	20 (25.3)	20 (25.3)	17/20 (85.0)	31 (38.3)	31 (38.3)	29/31 (93.5)
	Round	2 (2.5)	1 (1.3)	1/1 (100.0)	9 (11.1)	8 (9.9)	8/8 (100.0)
	Irregular	57 (72.2)	58 (73.4)	55/58 (94.8)	41 (50.6)	42 (51.9)	39/42 (92.9)
Margin	Circumscribed	1 (1.3)	0 (0.0)	0/0	4 (4.9)	3 (3.7)	3/3 (100.0)
	Not circumscribed	78 (98.7)	79 (100.0)	78/79 (98.7)	77 (95.1)	78 (96.3)	77/78 (98.7)
Internal enhancement (signal)	Homogeneous	2 (2.5)	0 (0.0)	0/0	1 (1.23)	1 (1.23)	1/1 (100.0)
	Heterogeneous	54 (68.4)	35 (44.3)	33/35 (94.3)	51 (63.0)	34 (42.0)	34/34 (100.0)
	High signal in rim shape	23 (29.1)	44 (55.7)	22/44 (50.0)	29 (35.8)	46 (56.8)	29/46 (63.0)
	Dark internal septations	0 (0.0)	0 (0.0)	0/0	0 (0.0)	0 (0.0)	0/0
Non-mass lesions		Reader A	N = 37		Reader B	N = 33	
		N (%)		N/CE[a] (%)	N (%)		N/CE[a] (%)
		DWI	CE	Number of agreements	DWI	CE	Number of agreements
Distribution	Focal	11 (29.7)	9 (24.3)	9/9 (100.0)	4 (12.1)	2 (6.0)	2/2 (100.0)
	Linear	2 (5.4)	2 (5.4)	1/2 (50.0)	4 (12.1)	3 (9.1)	3/3 (100.0)
	Segmental	23 (62.2)	25 (67.6)	23/25 (92.0)	24 (72.7)	27 (81.8)	24/27 (88.9)
	Regional	0 (0.0)	0 (0.0)	0/0	0 (0.0)	0 (0.0)	0/0
	Multiple regions	1 (2.7)	1 (2.7)	1/1 (100.0)	1 (3.0)	1 (3.0)	1/1 (100.0)
	Diffuse	0 (0.0)	0 (0.0)	0/0	0 (0.0)	0 (0.0)	0/0
Internal enhancement (signal)	Homogeneous	1 (2.7)	1 (2.7)	1/1 (100.0)	1 (3.0)	0 (0.0)	0/0
	Heterogeneous	14 (37.8)	9 (24.3)	7/9 (77.8)	7 (21.2)	6 (18.2)	4/7 (66.7)
	Clumped	21 (56.8)	21 (56.8)	17/21 (81.0)	25 (75.8)	18 (54.6)	17/18 (94.4)
	Clustered ring	1 (2.7)	6 (16.2)	1/6 (16.7)	0 (0.0)	9 (27.3)	0/9 (0.0)

[a] N/CE represents number of lesions with which the descriptors agreed on both methods / number of lesions detected on HR CE-MRI.

Table 4
Comparison and correlation between lesion diameters on HR-DWI and HR CE-MRI.

		Reader A		Reader B	
		HR-DWI	HR CE-MRI	HR-DWI	HR CE-MRI
Mass lesions	lesion size[a] (mm)	15.0 ± 9.7	17.3 ± 10.1 p = .035	15.7 ± 10.1	16.8 ± 9.6 p = .19
	Spearman's coefficient	0.90 (p < .0001)		0.96 (p < .0001)	
Non-mass lesions	lesion size[a] (mm)	19.5 ± 14.8	22.9 ± 14.8 p = .24	21.2 ± 13.5	25.6 ± 14.6 p = .20
	Spearman's coefficient	0.86 (p < .0001)		0.86 (p < .0001)	

[a] The number corresponds to mean and standard deviation.

of non-mass lesions. However, the agreement of internal signal/enhancement pattern [19] was not as good as the other subcategories either in mass or non-mass lesions. Size assessment showed very strong correlation between HR-DWI and HR CE-MRI both in mass lesions and in non-mass lesions.

There are only a few reports concerning the evaluation of morphology using DWI in breast lesions. While various levels of agreement between conventional DWI using ss-EPI and DCE-MRI have been reported in the evaluation of mass lesions [24,29,30], our study showed higher agreement in terms of shape and marginal evaluation using HR-DWI. As for non-mass lesions, very few reports have evaluated the morphology using HR-DWI, even with DWI using rs-EPI, as far as we know [24,30]. In that sense, our study shows the valuable data from the larger sample size, including non-mass lesions.

A high degree of agreement between HR-DWI and HR CE-MRI in mass lesion size was demonstrated in our study. The excellent agreement between HR-DWI and pathology of the malignant lesions were observed in our previous study [19]. These results can be attributed to the nearly-isovoxel high spatial resolution unique to our protocol and indicate the potential to substitute contrast-enhanced MRI with HR-DWI. Our study also showed excellent agreement in HR-DWI and HR CE-MRI for lesion margins.

The differences in the assessment of morphology in mass lesions were mostly seen in the “internal enhancement/signals”. The lesions assessed to have “high signal in rim shape” on HR-DWI showed high agreement with those on HR CE-MRI, however, slightly more than half of the lesions with rim enhancement were not assessed “high signal in rim shape”, but as “heterogeneous signal” on HR-DWI. The suspicious morphologic features for malignancy were irregular/spiculated margin with rim or heterogeneous internal enhancement [4,5,31]. Distinguishing rim from heterogeneous signal/enhancement was sometimes difficult on HR-DWI in our study; however, neither reader assessed these findings as “homogeneous” or “dark internal septations”, meaning they at least interpreted that the lesions had malignant features.

Our study showed a good correlation between HR-DWI and HR CE-MRI in non-mass lesion size. As for morphology, even with the high resolution of our study, “clustered-ring signals” (internal enhancement) was difficult to identify. Clumped enhancement on HR CE-MRI showed relatively high agreement with HR-DWI; still the agreement among heterogeneous, clumped or clustered-ring patterns was variable. Non-mass lesions with segmental and linear distribution, as well as clustered-ring and clumped enhancement, were previously reported to have the highest positive predictive value for malignancy [5,31,32], meaning HR-DWI has the potential to be applied or at least add value to the evaluation of breast cancer using BI-RADS descriptors. Now that BI-RADS MRI has been established for the morphological assessment of breast lesions, it is valuable to utilize the same lexicon for HR-DWI in the daily clinical settings.

The certain features in BI-RADS showed high agreement between HR-DWI and HR CE-MRI, which may be explained by the fact that breast malignant lesions share characteristics of restricted diffusion or abnormal enhancement compared to the surrounding tissue. On the other hand, the lower agreement which is seen in “internal enhancement/signals” in both mass and non-mass lesions may be due to the two methods referring to different tissue properties; one focused on tissue permeability while the other focused on cell density. Similarly, Kang et al. reported that no correlation was observed between the DCE-MRI and DWI rim signs [33]. The difference in voxel size between two methods may be one of the reasons for the lower agreement. Higher resolution maintaining low distortion may provide more detailed evaluation of the internal enhancement. Our previous study showed that almost 50% of non-mass lesions were not detected [19], suggesting that detection of non-mass lesion on DWI could be improved.

Our study has several limitations. First, this was a retrospective

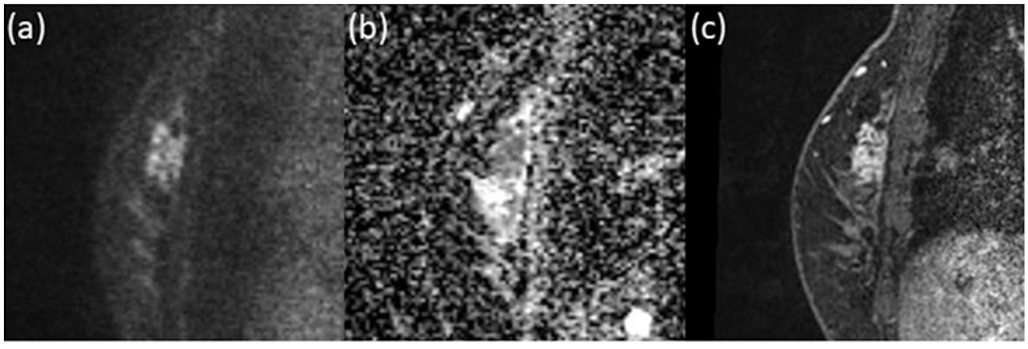

Fig. 4. Malignant non-mass lesion in a 47-year-old patient.
(a) HR-DWI (b = 850 s/mm^2), (b) ADC map, (c) HR CE-MRI.
(a, b) Non-mass lesion with high intensity on HR-DWI (b = 850 s/mm^2) with low values on ADC map was detected. (c) The lesion was detected on HR CE-MRI.
Both readers classified it as a non-mass lesion on both methods. Reader A measured it as 11 mm on HR-DWI and 14 mm on HR CE-MRI, while reader B measured it as 12 mm on HR-DWI and 14 mm on HR CE-MRI. Both readers diagnosed the lesion with segmental distribution, and reader A diagnosed a clustered ring pattern while reader B diagnosed a heterogeneous signal pattern on HR-DWI. Both readers diagnosed the lesion with segmental distribution with clustered ring enhancement on HR CE-MRI. The pathological diagnosis was intermediate-grade DCIS.

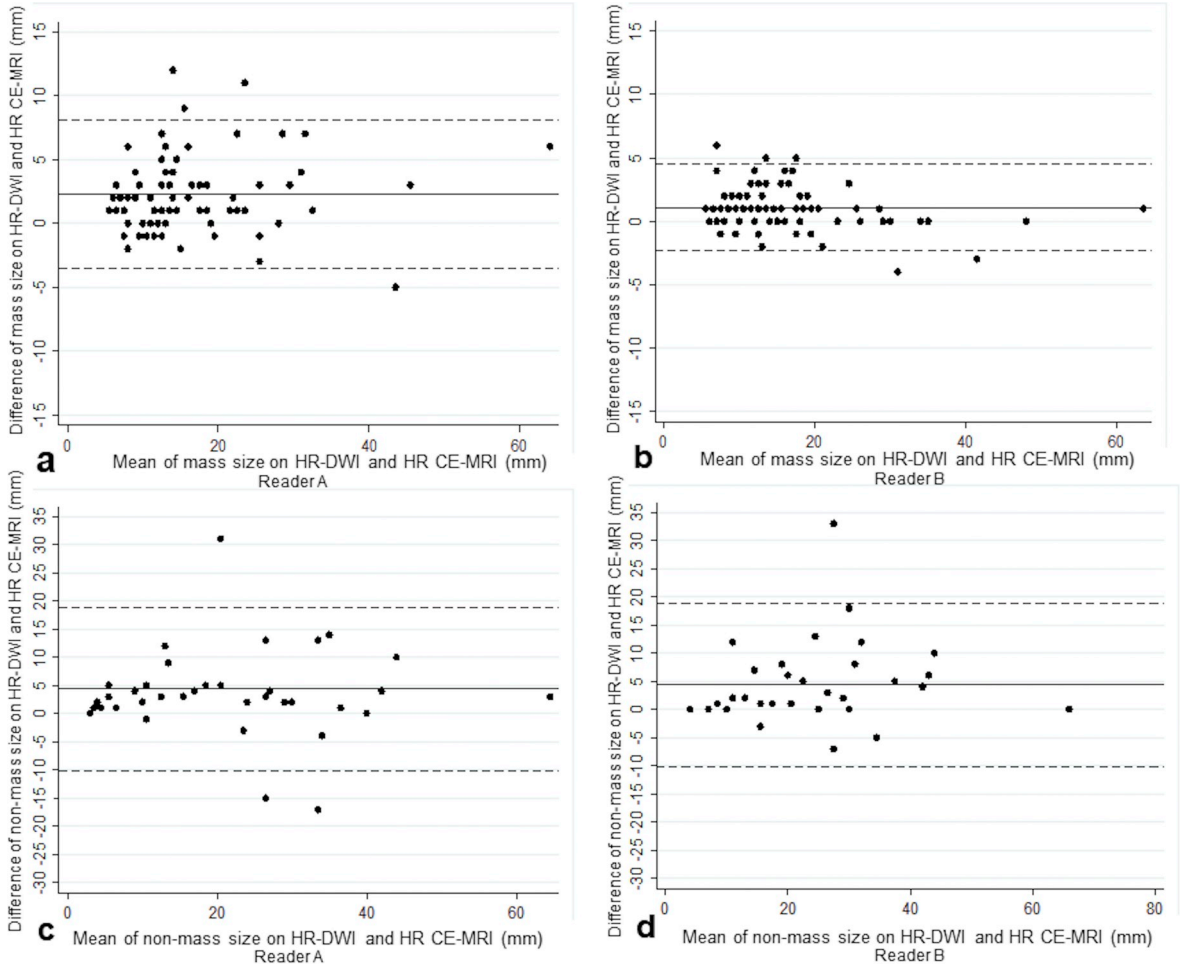

Fig. 5. Bland-Altman plots of agreement between lesion diameters measured on HR-DWI and on HR CE-MRI by two readers, regarding mass lesions (a, b), and non-mass lesions (c, d). The horizontal straight line and the two dotted lines above/below it indicates the mean difference plus and minus 1.96 times the standard deviation of the differences respectively. Mass lesions showed higher concordance correlation compared to non-mass lesions.

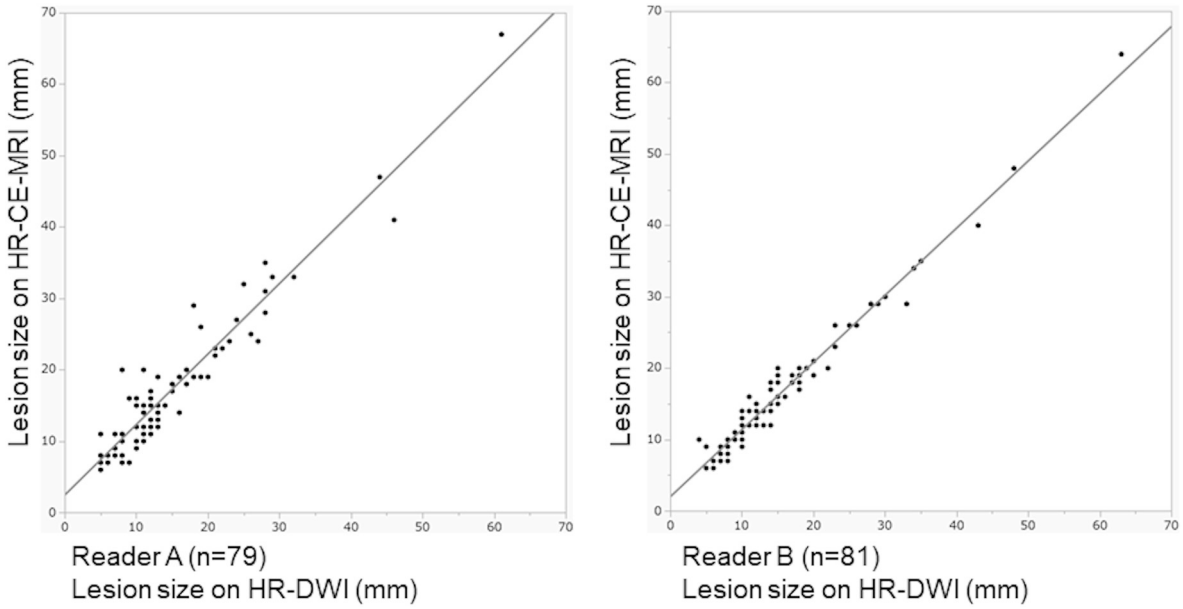

Fig. 6. Scatterplot showing the correlation between diameters of mass lesions on HR-DWI and HR CE-MRI.
Reader A detected 79 mass lesions and reader B detected 81 mass lesions.

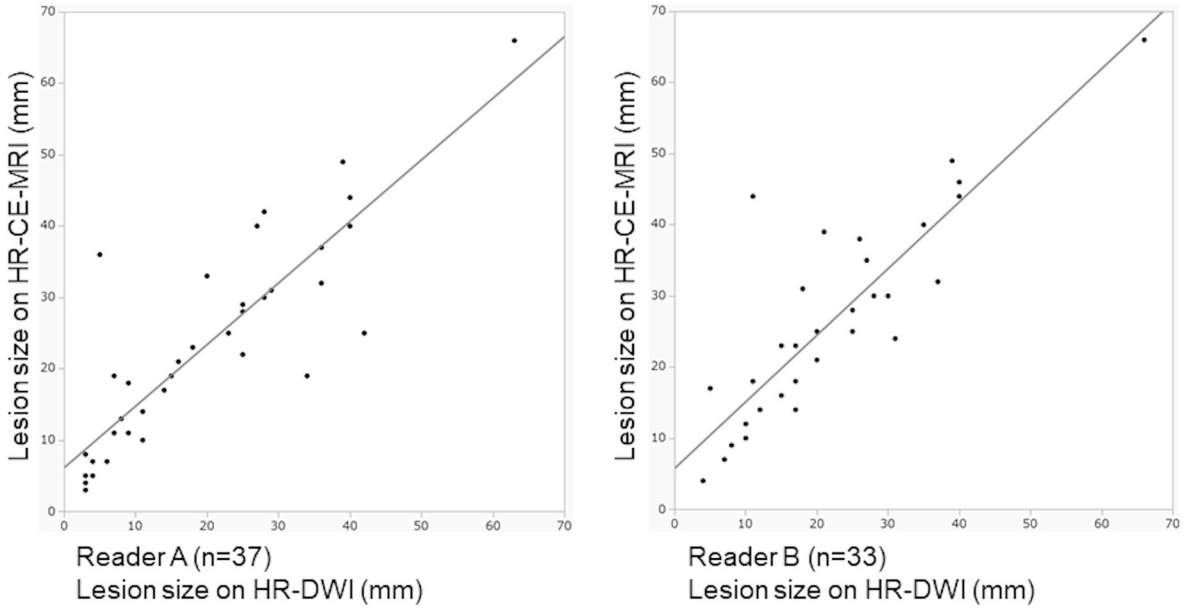

Fig. 7. Scatterplot showing the correlation between diameters of non-mass lesions on HR-DWI and HR CE-MRI. Reader A detected 37 non-mass lesions and reader B detected 33 non-mass lesions.

study with a preliminary investigation of a limited number of breast lesions. Second, only cases with malignant lesions were included, thus the cancer prevalence is different from daily clinical situations, which may cause potential bias and limit generalizability. Third, since we have not compared lesion size on images with pathology, no stratification of results by lesion size on pathological character has been obtained. Fourth, the lower resolution in HR-DWI compared to HR CE-MRI may underestimate the agreement in size or BI-RADS features in two methods. We have also acquired DWI using b value with 850 s/mm^2, which were determined as an optimal value to achieve reasonable resolution and SNR [18]. Acquiring higher b value might increase contrast-to-noise ratio; however, the recently published consensus paper has recommended b value of 800 s/mm^2, which almost aligns with our study [34].

5. Conclusions

HR-DWI using rs-EPI showed agreement in morphology and lesion extent estimation on HR CE-MRI. These results imply the potential of applying HR-DWI to evaluation of malignant breast lesions using BI-RADS descriptors.

CRediT authorship contribution statement

Ayami Ohno Kishimoto: Conceptualization, Methodology, Validation, Formal analysis, Investigation, Resources, Data curation, Writing - original draft, Writing - review & editing, Visualization. **Masako Kataoka:** Conceptualization, Methodology, Validation, Formal analysis, Writing - review & editing, Supervision, Project administration. **Mami Iima:** Conceptualization, Methodology, Validation, Formal analysis, Writing - review & editing, Supervision, Project administration. **Maya Honda:** Validation, Data curation, Writing - review & editing. **Kanae Kawai Miyake:** Validation, Writing - review & editing. **Akane Ohashi:** Data curation, Writing - review & editing. **Rie Ota:** Data curation, Writing - review & editing. **Tatsuki Kataoka:** Data curation, Writing - review & editing. **Takaki Sakurai:** Data curation, Writing - review & editing. **Masakazu Toi:** Data curation, Writing - review & editing. **Kaori Togashi:** Writing - review & editing, Supervision, Project administration.

Acknowledgment

We thank Dr. Libby Cone, from Edanz Group Japan for editing drafts of this manuscript.

We thank Mr. Yuta Urushibata from Siemens Healthcare K.K. for the technical support in this work.

Funding

This research did not receive any specific grant from funding agencies in the public, commercial, or not-for-profit sectors.

Declaration of competing interest

None.

References

[1] Morris EACC, Lee CH, et al. ACR BI-RADS® magnetic resonance imaging. ACR BI-RADS® atlas, breast imaging reporting and data system. Reston, VA: American College of Radiology; 2013.
[2] Rahbar H, Partridge SC. Multiparametric MR imaging of breast cancer. Magn Reson Imaging Clin N Am 2016;24(1):223–38.
[3] Schnall MD, Blume J, Bluemke DA, DeAngelis GA, DeBruhl N, Harms S, et al. Diagnostic architectural and dynamic features at breast MR imaging: multicenter study. Radiology 2006;238(1):42–53.
[4] Bluemke DA, Gatsonis CA, Chen MH, DeAngelis GA, DeBruhl N, Harms S, et al. Magnetic resonance imaging of the breast prior to biopsy. JAMA 2004;292(22):2735–42.
[5] Goto M, Ito H, Akazawa K, Kubota T, Kizu O, Yamada K, et al. Diagnosis of breast tumors by contrast-enhanced MR imaging: comparison between the diagnostic performance of dynamic enhancement patterns and morphologic features. J Magn Reson Imaging 2007;25(1):104–12.
[6] Kuhl CK, Schild HH, Morakkabati N. Dynamic bilateral contrast-enhanced MR imaging of the breast: trade-off between spatial and temporal resolution. Radiology 2005;236(3):789–800.
[7] Sadowski EA, Bennett LK, Chan MR, Wentland AL, Garrett AL, Garrett RW, et al. Nephrogenic systemic fibrosis: risk factors and incidence estimation. Radiology 2007;243(1):148–57.
[8] Kang H, Hii M, Le M, Tam R, Riddehough A, Traboulsee A, et al. Gadolinium deposition in deep brain structures: relationship with dose and ionization of linear gadolinium-based contrast agents. Am J Neuroradiol 2018;39(9):1597–603.
[9] Layne KA, Dargan PI, Archer JR, Wood DM. Gadolinium deposition and the potential for toxicological sequelae–a literature review of issues surrounding gadolinium-based contrast agents. Br J Clin Pharmacol 2018;84(11):2522–34.
[10] Kanda T, Ishii K, Kawaguchi H, Kitajima K, Takenaka D. High signal intensity in the dentate nucleus and globus pallidus on unenhanced T1-weighted MR images:

relationship with increasing cumulative dose of a gadolinium-based contrast material. Radiology 2013;270(3):834–41.
[11] Errante Y, Cirimele V, Mallio CA, Di Lazzaro V, Zobel BB, Quattrocchi CC. Progressive increase of T1 signal intensity of the dentate nucleus on unenhanced magnetic resonance images is associated with cumulative doses of intravenously administered gadodiamide in patients with normal renal function, suggesting dechelation. Invest Radiol 2014;49(10):685–90.
[12] Shi RY, Yao QY, Wu LM, Xu JR. Breast lesions: diagnosis using diffusion weighted imaging at 1.5T and 3.0T-systematic review and meta-analysis. Clin Breast Cancer 2018;18(3). (e305-e20).
[13] Zhang L, Tang M, Min Z, Lu J, Lei X, Zhang X. Accuracy of combined dynamic contrast-enhanced magnetic resonance imaging and diffusion-weighted imaging for breast cancer detection: a meta-analysis. Acta Radiol 2016;57(6):651–60.
[14] Partridge SC, DeMartini WB, Kurland BF, Eby PR, White SW, Lehman CD. Quantitative diffusion-weighted imaging as an adjunct to conventional breast MRI for improved positive predictive value. Am J Roentgenol 2009;193(6):1716–22.
[15] Woodhams R, Ramadan S, Stanwell P, Sakamoto S, Hata H, Ozaki M, et al. Diffusion-weighted imaging of the breast: principles and clinical applications. RadioGraphics 2011;31(4):1059–84.
[16] Porter DA, Calamante F, Gadian DG, Connelly A. The effect of residual Nyquist ghost in quantitative echo-planar diffusion imaging. Magn Reson Med 1999;42(2):385–92.
[17] Delbany M, Bustin A, Poujol J, Thomassin-Naggara I, Felblinger J, Vuissoz P-A, et al. One-millimeter isotropic breast diffusion-weighted imaging: evaluation of a superresolution strategy in terms of signal-to-noise ratio, sharpness and apparent diffusion coefficient. Magn Reson Med 2019;81(4):2588–99.
[18] Kanao S, Kataoka M, Iima M, Ohno A, Sakaguchi R, Ohashi A, et al. High-resolution diffusion-weighted MRI of the breast using readout-segmented EPI and single-shot EPI. Imaging Med 2017;9(6):185–90.
[19] Kishimoto AO, Kataoka M, Iima M, Togashi K, et al. Evaluation of malignant breast lesions with high-resolution diffusion-weighted imaging using readout-segmented echo-planar imaging: comparison with pathology. Magn Reson Med Sci 2020. Japanese Society for Magnetic Resonance in Medicine; In press.
[20] Iima M, Yamamoto A, Brion V, Okada T, Kanagaki M, Togashi K, et al. Reduced-distortion diffusion MRI of the craniovertebral junction. Am J Neuroradiol 2012;33(7):1321–5.
[21] Koyasu S, Iima M, Umeoka S, Morisawa N, Porter DA, Ito J, et al. The clinical utility of reduced-distortion readout-segmented echo-planar imaging in the head and neck region: initial experience. Eur Radiol 2014;24(12):3088–96.
[22] Bogner W, Pinker-Domenig K, Bickel H, Chmelik M, Weber M, Helbich TH, et al. Readout-segmented echo-planar imaging improves the diagnostic performance of diffusion-weighted MR breast examinations at 3.0 T. Radiology 2012;263(1):64–76.
[23] Baltzer PA, Bickel H, Spick C, Wengert G, Woitek R, Kapetas P, et al. Potential of noncontrast magnetic resonance imaging with diffusion-weighted imaging in characterization of breast lesions: intraindividual comparison with dynamic contrast-enhanced magnetic resonance imaging. Invest Radiol 2018;53(4):229–35.
[24] An YY, Kim SH, Kang BJ. Differentiation of malignant and benign breast lesions: added value of the qualitative analysis of breast lesions on diffusion-weighted imaging (DWI) using readout-segmented echo-planar imaging at 3.0 T. PLoS One 2017;12(3):e0174681.
[25] Kataoka M, Kanao S, Iima M, Onishi N, Kawai M, Ohashi A, et al. High resolution DWI with readout-segmented EPI and computed DWI as a potential alternative of high resolution dynamic contrast enhanced MRI in evaluating breast cancer. Proc Int Soc Magn Reson Med 2016;24.
[26] Viera AJ, Garrett JM. Understanding interobserver agreement: the kappa statistic. Fam Med 2005;37(5):360–3.
[27] Chan Y. Biostatistics 104: correlational analysis. Singapore Med J 2003;44(12):614–9.
[28] Feinstein AR, Cicchetti DV. High agreement but low kappa: I. the problems of two paradoxes. J Clin Epidemiol 1990;43(6):543–9.
[29] Kul S, Metin Y, Kul M, Metin N, Eyuboglu I, Ozdemir O. Assessment of breast mass morphology with diffusion-weighted MRI: beyond apparent diffusion coefficient. J Magn Reson Imaging 2018;48(6):1668–77.
[30] Radovic N, Ivanac G, Divjak E, Biondic I, Bulum A, Brkljacic B. Evaluation of breast cancer morphology using diffusion-weighted and dynamic contrast-enhanced MRI: intermethod and interobserver agreement. J Magn Reson Imaging 2019;49(5):1381–90.
[31] Liberman L, Morris EA, Lee MJ-Y, Kaplan JB, LaTrenta LR, Menell JH, et al. Breast lesions detected on MR imaging: features and positive predictive value. Am J Roentgenol 2002;179(1):171–8.
[32] Tozaki M, Fukuda K. High-spatial-resolution MRI of non-masslike breast lesions: interpretation model based on BI-RADS MRI descriptors. Am J Roentgenol 2006;187(2):330–7.
[33] Kang BJ, Lipson JA, Planey KR, Zackrisson S, Ikeda DM, Kao J, et al. Rim sign in breast lesions on diffusion-weighted magnetic resonance imaging: diagnostic accuracy and clinical usefulness. J Magn Reson Imaging 2015;41(3):616–23.
[34] Baltzer P, Mann RM, Iima M, Sigmund EE, Clauser P, Gilbert FJ, et al. Diffusion-weighted imaging of the breast—a consensus and mission statement from the EUSOBI International Breast Diffusion-Weighted Imaging working group. Eur Radiol 2019:1–15.